Compressive behaviour of a square origami surface-based lattice structure fabricated by selective laser melting

Jian Gao[1], Quanquan Han[1*], Shwe Soe[2*], Zhongyi Liu[1], Jiafeng Feng[3], Zhenhua Zhang[1], Liqiao Wang[1]

[1] Key Laboratory of High Efficiency and Clean Mechanical Manufacture of Ministry of Education, School of Mechanical Engineering, Shandong University, Jinan, 250061, China
[2] Department of Engineering, Design and Mathematics, University of the West of England, Bristol BS16 1QY, UK
[3] School of Automotive Engineering, Weifang Vocational College, Weifang, 262737, China

Corresponding author:
Quanquan Han, hanquanquan@sdu.edu.cn, +86531-88392608
Shwe Soe, shwe.soe@uwe.ac.uk,

Abstract.
Selective laser melting (SLM) is a metal additive manufacturing process that shows significant advantages in manufacturing lattice structures. In this paper, a novel surface-based square origami structure made of a nickel-based superalloy was fabricated using SLM. Three different wall thicknesses (50, 75 and 100 μm) were used to examine the manufacturability and corresponding compressive behaviour of the manufactured lattice components. Finite element analysis (FEA) was conducted to determine the uniaxial compression and then verified by quasi-static compression testing. The results showed that the components with thinner walls more easily folded and buckled than those with thicker walls, indicating that higher densification strains and energy absorption values may be achieved with thinner walls, although the thicker walls were stronger and could withstand larger loads. This research offers insights into the design and manufacture of advanced lattice structures by providing an improved understanding of the compressive behaviour of surface-based square origami structures.

Keywords: Additive manufacturing, Cellular, Simulation, Strength.

1   Introduction

The lattice structure is a porous formation composed of unit cells arranged periodically in a three-dimensional space. These porous structures offer many advantages, including lightness and high specific strength/stiffness. Because lattice structures are mostly hollow and complex-shaped, fabricating such structures by traditional processing methods is very challenging. The selective laser melting (SLM) process is an additive manufacturing (AM) technology in which a high-powered laser is used to selectively melt pow-

der from bottom to top according to a computer-aided design (CAD) model. The process is quite accurate for forming and, in theory, can be used to manufacture metallic parts with any complex shapes [1]. Compared to other metal AM processes such as electron beam melting and direct metal deposition, SLM offers improved forming accuracy and thus is more suitable for processing lattice structures [2].

Because of its good compression, shock-absorption and energy-absorption performance, the honeycomb structure is widely used in the aerospace sector and further afield [3]. Due to its peculiarity of lightweight, aluminum alloy and titanium alloy have been studied extensively and made into a range of honeycomb structures [4]. However, there are scant studies on the manufacturability and mechanical performance of different lattice configurations in nickel-based super alloy possessing excellent oxidation and corrosion resistance [5]. Since light weighting and energy-absorption performance are highly associated to the design and fabrication of lattices with the least material possible, the research question lies on the overall quality (accuracy, surface roughness, and mechanical properties) of minimum wall thicknesses (i.e. < 1 mm) that can be successfully manufactured in SLM process.

In the present research, a surface-based square origami structure was manufactured via SLM using nickel-based superalloy material, in order to test the possibility of fabricating very thin walls (< 1mm) and the corresponding compressive behavior. The structure had to be lightweight and strong and show good compression for potential use in the aerospace field, in additional to displaying good shock- and energy-absorption values. To capture the mechanical response under load, quasi-static compression tests were conducted on square origami structures with different wall thicknesses and its buckling and collapse behavior were recorded using a high-resolution camera. Finite element analysis (FEA) was employed to inform the validity of computational and experimental compression responses of square origami structures with different wall thicknesses.

2   Materials and methods

2.1   Design of the square origami structure

The lattice structure used in this study is composed of unit cells arranged along an X shape. The unit cell (see Fig. 1a), composed of trapezoidal thin walls (upper bottom: 8 mm; lower bottom: 12 mm), has a rectangular hollow structure (length: 12 mm; width: 8 mm). Three different wall thicknesses of 50 μm, 75 μm and 100 μm were designed to have the relative densities of 0.09, 0.13 and 0.18, respectively. In the build direction, the origami structure consists of three rows of unit cells, each 10 mm high, with a total height of 30 mm.

The isometric view of the sample (see Fig. 1b) shows the origami structure is a cube. Note that the trapezoidal thin-walled structure is symmetrical, and the area where the thin outermost adjacent trapezoidal walls are in contact with the hypotenuse is a band with a spacing of 1 mm. The reason of designing the band shape is to remove the shape edges of the origami structure, where the stress concentration normally occurs during the compression process [6]. In other word, the band shape is designed to achieve a

good connectivity between lattices, such that the square origami structure can absorb more energy.
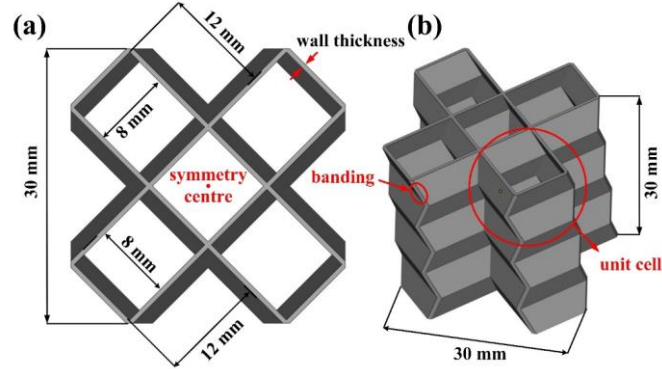
Fig. 1. CAD model of a square origami structure: (a) top view; (b) isometric view.

2.2 Numerical modeling setup

FEA was conducted to understand the stress-strain distribution of the square origami structures during the quasi-static compression process. For FEA, the three above-mentioned CAD geometries with different wall thicknesses were imported into Abaqus as STEP files and compression models. The material used in this experiment is a nickel-based superalloy. Before this compression testing, tensile samples of the nickel-based superalloy were fabricated using SLM. The tensile testing was conducted at room temperature of 25 °C. According to the tensile test data, the elasto-plastic material model was calibrated using Abaqus's calibration tool; the Young's modulus and Poisson's ratio were set to 150.81 GPa, and 0.33. Isotropic plastic hardening model was established with sufficient data points in a tabulated format. Tensile testing was first simulated during the Abaqus FEA to ensure the accuracy of the simulation parameter settings of the compression experiment.
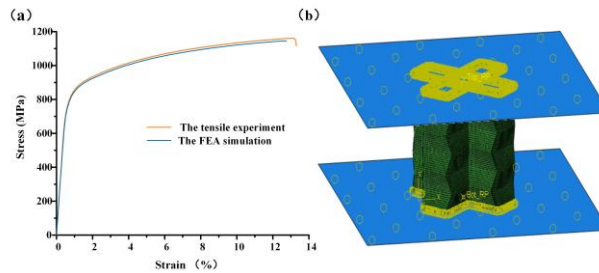
Fig. 2. (a) Stress-strain curve of tensile experiment and FEA simulation; (b) simulation model for the FEA compression experiment.

As shown in Fig. 2a, the simulated stress-strain curve was very close to that of the tensile experiment, so the parameters set by the Abaqus FEA provided reasonable fidelity. In the lattice modelling set up, rigid plates are added as boundary conditions to the top and bottom of the model, and each model, finely meshed with C3D8R linear hexahedral elements, was constrained between the analytical rigid surfaces, as shown in Fig. 2b. The general contact condition was imposed for self-interaction. To sustain computational efficiency and robustness Abaqus dynamic explicit solver was employed. During compression the reference point fixed at the centre of the top surface was allowed to move axially when the bottom surface was fully fixed. The reaction force and displacement values, extracted through the described reference point, were translated into compressive stress and strain data. The damaged model with a fracture strain limit, which was mapped to the experimental data, enabled capturing the potential material fracture at the highly stressed regions.

2.3   Selective laser melting progress

The material used in this study – a strong, nickel-based superalloy, with good mechanical properties and high-temperature oxidation resistance. The elemental composition of nickel-based superalloys was (wt.%) 22.37Cr-14.05W-2Mo-0.51Si-0.49Mn-0.37Al-0.3Fe-0.11C-Bal. The samples were manufactured using an Mlab cusing 200R SLM (Concept Laser GmbH, Germany), equipped with a 200 W continuous wave fiber laser (Table 1).

Table 1. Process parameters for manufacturing origami structure via SLM

Laser power	Scanning speed	Layer thickness	Hatch spacing
200 W	800 mm/s	40 µm	110 µm

Three kinds of square origami structures with different wall thicknesses (50, 75 and 100 μm) were fabricated to study the effect of wall thickness on the compression performance of the square origami structure (Fig. 3).
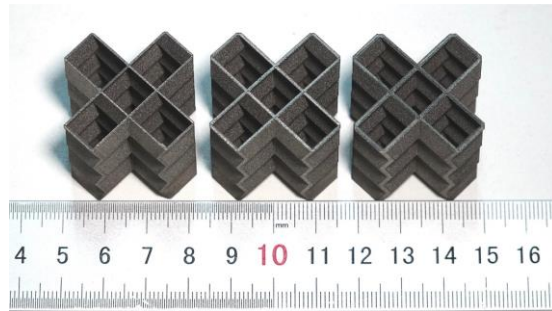
Fig. 3. Manufactured square origami structures (50, 75 and 100 μm).

2.4 Quasi-static compression testing

Quasi-static compression testing was performed using a universal testing machine (Z250) produced by ZwickRoell, Germany. The compression samples were divided into three groups according to the wall thickness (50, 75 and 100 μm), and each group had three samples to ensure the stability of quasi-static compression test and the reliability of compression test data. The compression rate was set to 2 mm/min for all compression tests. The compression process was recorded by a high-resolution camera to record compression moments to better analyse the failure-deformation behaviour of the square origami structures.

3 Results and discussion

3.1 Finite element analysis

Fig. 4 shows stress-distribution clouds of the three kinds of square origami structures with different wall thicknesses during quasi-static compression via FEA. In the process of compression simulation, the stress concentration occurred in the middle folding area for the origami structure with a wall thickness of 50 μm, which also led to lower compressive strength and stiffness values. The origami structures with thicker walls experienced more uniform stress distribution across all folding regions during compression testing. The corresponding compressive strain values (%) for the displacement at (1, 2, 3.8 and 5 mm) can be interpreted as (3.3, 6.6, 12.7 and 16.6) respectively.
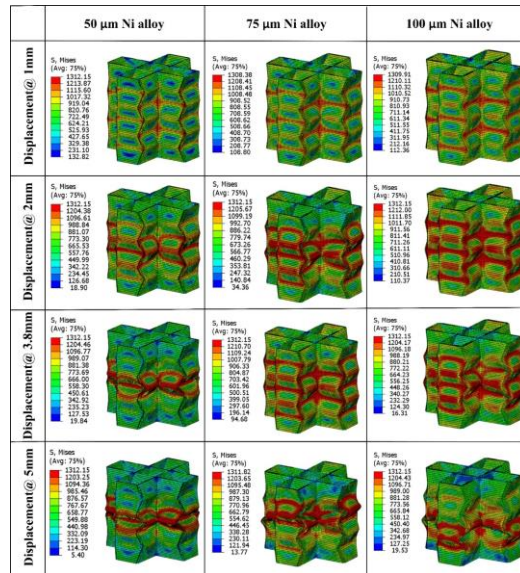
Fig. 4. Stress-distribution clouds for FEA compression simulation of three kinds of origami structures with different wall thicknesses.

Fig. 5 shows corresponding strain-distribution clouds of the three kinds of square origami structures. In the process of compression simulation, with increased compression displacement, the strain was also found to be evenly distributed in the folding area, which implied that the square origami structure has a good effect of shock- and energy-absorption. The stress-strain distribution simulation results in Fig. 4 and Fig. 5 reveal that the square origami structure with different wall thickness shows progressive damage during the compression process. Compared to the compressive direction, the stress and strain are mainly concentrated in the folding area of the square origami structure.
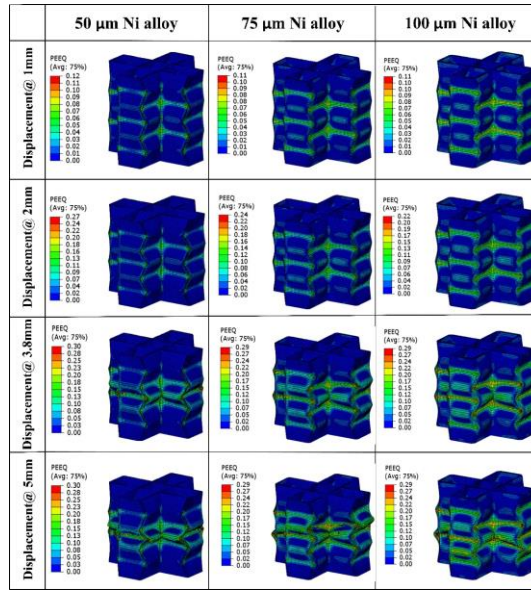
Fig. 5. Strain-distribution clouds for FEA compression simulation of three kinds of origami structures with different wall thicknesses.

Fig. 6 shows the stress histogram of the square origami structure with different compression displacements. Notably, when the compression displacement reached 3.8 mm, the stress on the origami structure with different wall thicknesses values significantly reduced. It may be concluded that during the stage of compression displacement between 2 and 3.8 mm, the square origami structure changed from the plateau stress stage to the failure stage, and the square origami structure may form cracks initiation and expansion during this stage. As the compression displacement further increased to 5 mm, the microscopic cracks further expanded and eventually caused the failure of the square origami structure.
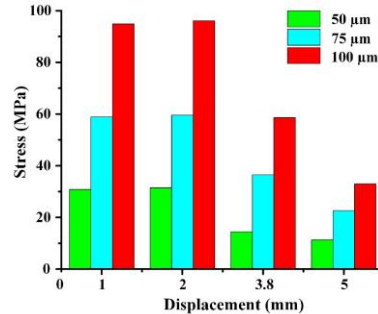
Fig. 6. FEA simulated stress diagram under different compression displacements of three kinds of origami structures with different wall thickness values.

3.2 Experimental results

Quasi-static compression testing results

Fig. 7 shows the quasi-static compressive stress-strain curves from experiment and Abaqus FEA of three kinds of square origami structures with different wall thicknesses. The compression curves of the three structures were found to show similar trends, which could be divided into three stages:

In the linear growth stage (0-1.5%), the stress-strain curve was approximately a straight line, and the relationship between stress and strain showed a linear relationship, which reflects the strength performance of nickel-based superalloy materials.
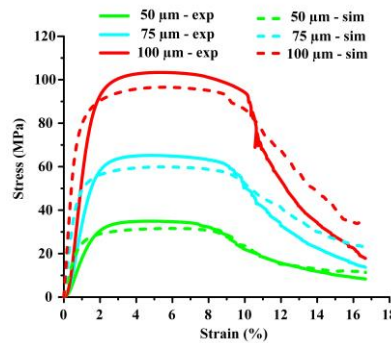
Fig. 7. Stress-strain curve diagram of experimentation and FEA for three kinds of square origami structures with different wall thicknesses.

In the second stage (1.5-10%), the stress-strain curve tended to be stable, with a plateau period. In this stage, with increased stress, the square origami structure lost its stability, and folding took place. The amount of deformation along the compression direction continued to increase, and the strain gradually increased. During the compression

testing, the energy absorption per unit volume of the square origami structure could be calculated by the following equation [6]:

$$W_V = \int_0^{\varepsilon} \sigma(\varepsilon)d\varepsilon$$

(1)

where W_v represents the absorbed energy per unit volume, ε is the strain, and $\sigma(\varepsilon)$ represents the corresponding stress.

In the plateau stage, the strain limits of the square origami structures with different wall thicknesses (50 μm, 75 μm and 100 μm) were 7%, 9% and 10%, respectively. The results showed that the origami structures with thinner walls were easier to fold and buckle, indicating that higher densification strains and energy absorption values may be achieved with thinner walls, although the thicker walls were stronger and could withstand larger loads. Consequently, the results offered insights into the design and manufacture of advanced lattice structures by providing an improved understanding of the compressive behaviour of surface-based square origami structures. Note that the maximum strain value of the square origami structure was only 10%, while the maximum strain value of other nickel-based superalloys in the literature could reach 30% [7,8], which indicated that the nickel-based superalloy used in this study was quite brittle.

Notably, the stress-strain curves obtained by compression experimentation and FEA were generally consistent, but the compressive stress values obtained by experimentation were slightly higher than the values obtained by simulation. From the perspective of FEA, the convergence of the mesh would lead to the simulation data higher than the experimental data. However, this study evaluated both shell and FEA modeling strategies whilst conducting a mesh convergence study to ensure that the extracted data was robust and reliable to be presented. From the perspective of plastic theory, the tensile stress-strain curve and compressive stress-strain curve of a material should be consistent [9]. As previous studies have revealed, however, the plastic deformation ability of metal materials under different stress states is not the same, and the stress-strain curve under compression is generally higher than that under tension [10]. In this study, the tensile test data were used as the input for the FEA model as the material properties of the nickel-based superalloy, which may explain why the experimental results were different from the simulation results. Also, the size of the CAD model of the origami structure was idealized in this study, and during the actual SLM process, the surface roughness of the lattice structure could be affected by the size of the laser spot, the quality of the powder bed and other factors, resulting in larger dimensional accuracy of the lattice structure, which may also cause the experimental value of quasi-static compression stress-strain curve to be higher than the FEA simulation results.

Damage and deformation mechanisms
The whole experimental process was recorded with a high-resolution camera during compression testing to better reveal the damage and deformation mechanisms of square origami structures with different wall thicknesses (50 μm, 75 μm and 100 μm) (Fig. 8).

At the beginning of compression (with compression displacement 1–2 mm and corresponding strain 3.3%–6.6%), the square origami structure was in a stage of linear

growth of stress and strain. At this stage, the stress was evenly distributed in the folding area of the square origami structure. When the compression displacement reached 3 mm, the stress was mainly distributed in the folding area near the centre of the square origami structure. During the third stage of the compression process, the stress concentration in the folding area of the central position was very high, which led to instability in the central folding area of the square origami structure. The folding area began to crack, and finally fracture failure occurred.
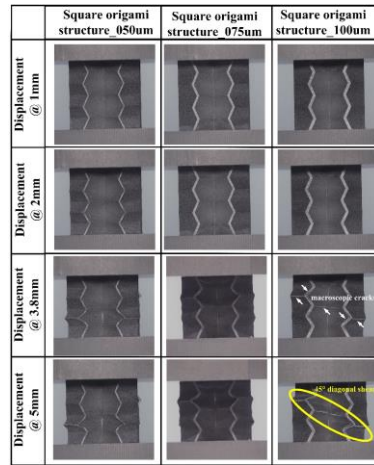
Fig. 8. Deformation behaviour of the square origami structure during quasi-static compression.

4 Conclusions

In this study we have developed a new square origami structure made of a nickel-based superalloy, manufactured with different wall thicknesses by the selective laser melting (SLM) process. Based on the results of finite element analysis (FEA) and experimentation, the main findings are as follows:

(1) The FEA simulation results showed that during the quasi-static compression process, the stress was evenly distributed in the folding area of the origami structure, indicating that this structure exhibited good load-bearing capacity.

(2) Before the square origami structure cracked and failed in the folding area, a plateau period occurred during the testing, indicating that this new square origami structure displayed good shock- and energy-absorption performance. In particular, the lattice structure with the thinnest wall (50 μm) was found to have the best energy-absorption performance under low stress. The nickel-based alloy used in the experiment was fairly brittle, however, which was also the main reason for the decreased stress found in the stress-strain curve.

(3) The results of the present study indicate that the SLM process may be used with advanced lattice structures made of nickel-based superalloys to accelerate the design of applications intended for lightweight structural performance.

10

References

[1]   Q. Han, H. Gu, S. Soe, R. Setchi, F. Lacan, J. Hill, Manufacturability of AlSi10Mg overhang structures fabricated by laser powder bed fusion, Mater. Des. 160 (2018) 1080–1095. https://doi.org/10.1016/J.MATDES.2018.10.043.

[2]   S. Santosa, T. Wierzbicki, Crash behavior of box columns filled with aluminum honeycomb or foam, Comput. Struct. 68 (1998) 343–367. https://doi.org/10.1016/S0045-7949(98)00067-4.

[3]   A. Ataee, Y. Li, M. Brandt, C. Wen, Ultrahigh-strength titanium gyroid scaffolds manufactured by selective laser melting (SLM) for bone implant applications, Acta Mater. 158 (2018) 354–368. https://doi.org/10.1016/j.actamat.2018.08.005.

[4]   T. Maconachie, M. Leary, B. Lozanovski, X. Zhang, M. Qian, O. Faruque, M. Brandt, SLM lattice structures: Properties, performance, applications and challenges, Mater. Des. 183 (2019) 108137. https://doi.org/10.1016/J.MATDES.2019.108137.

[5]   Q. Han, Y. Gu, R. Setchi, F. Lacan, R. Johnston, S.L. Evans, S. Yang, Additive manufacturing of high-strength crack-free Ni-based Hastelloy X superalloy, Hast. Manuf. 30 (2019) 100919. https://doi.org/10.1016/j.addma.2019.100919.

[6]   Z. Alomar, F. Concli, Compressive behavior assessment of a newly developed circular cell-based lattice structure, Mater. Des. 205 (2021) 109716. https://doi.org/10.1016/j.matdes.2021.109716.

[7]   F. Chen, Q. Wang, C. Zhang, Z. Huang, M. Jia, Q. Shen, Microstructures and mechanical behaviors of additive manufactured Inconel 625 alloys via selective laser melting and laser engineered net shaping, J. Alloys Compd. 917 (2022) 165572. https://doi.org/10.1016/J.JALLCOM.2022.165572.

[8]   M. Leary, M. Mazur, H. Williams, E. Yang, A. Alghamdi, B. Lozanovski, X. Zhang, D. Shidid, L. Farahbod-Sternahl, G. Witt, I. Kelbassa, P. Choong, M. Qian, M. Brandt, Inconel 625 lattice structures manufactured by selective laser melting (SLM): Mechanical properties, deformation and failure modes, Mater. Des. 157 (2018) 179–199. https://doi.org/10.1016/J.MATDES.2018.06.010.

[9]   Y. Wang, X. Ren, Z. Chen, Y. Jiang, X. Cao, S. Fang, T. Zhao, Y. Li, D. Fang, Numerical and experimental studies on compressive behavior of Gyroid lattice cylindrical shells, Mater. Des. 186 (2020) 108340. https://doi.org/10.1016/J.MATDES.2019.108340.

[10]   V. Crupi, E. Kara, G. Epasto, E. Guglielmino, H. Aykul, Static behavior of lattice structures produced via direct metal laser sintering technology, Mater. Des. 135 (2017) 246–256. https://doi.org/10.1016/j.matdes.2017.09.003.